RSC Advances

PAPER

View Article Online
View Journal | View Issue

Cite this: *RSC Adv.*, 2022, **12**, 23754

Effective dispersion of oxidized multi-walled carbon nanotubes using a water-soluble *N,O*-carboxymethyl chitosan *via* non-covalent interaction†

Jinling Gao, * Tongtong Li, Mingzhe Song, Yuyao Zhao and Anxu Wang

Dispersible multi-walled carbon nanotubes (MWCNTs) in water have been widely applied in the nanotechnology field. This study reports a water-soluble *N,O*-carboxymethyl chitosan(*N,O*-CMCS) assisted individual dispersion of oxidized multi-walled carbon nanotubes (oMWCNTs) as a dispersant. First, the dispersing agent *N,O*-CMCS was successfully synthesized using the nucleophilic substitution of deacetylated chitosan with chloroacetic acid in an alkaline solution. It was further confirmed using Fourier transform infrared spectroscopy (FTIR). Second, after the treatment with the concentrated hydrochloric acid, the prepared oMWCNTs were dispersed in an aqueous solution of *N,O*-CMCS under ultrasonic vibrations. Finally, the dispersed aqueous solution was subjected to centrifugation to collect the supernatant of individually dispersed *N,O*-CMCS/oMWCNTs. In addition, transmission electron microscopy (TEM) further confirmed that the purity of oMWCNTs was improved after the acidification progress. Besides, the stability of the dispersion solution was evidenced by digital photos of oMWCNTs dispersed by *N,O*-CMCS before and after. Moreover, the UV-vis spectrum (the characteristic peak of dispersed oMWCNTs downshifted 13 nm) showed that the supernatant was enriched by the individual oMWCNTs. In particular, the analytical results of FTIR (the $-NH_2$ band of *N,O*-CMCS downshifted 7 cm^{-1}), resonance Raman spectroscopy (the I_D/I_G ratio of dispersed oMWCNTs only increased 0.14), and XRD identified the formation of a non-convalent interaction between *N,O*-CMCS and oMWCNTs. These findings reveal the dispersing nature of *N,O*-CMCS towards oMWCNTs in water media.

Received 10th June 2022
Accepted 16th August 2022

DOI: 10.1039/d2ra03592h

rsc.li/rsc-advances

1 Introduction

Multi-walled carbon nanotubes (MWCNTs) which are considered as an excellent material, are significant for all kinds of potential technological applications due to their exceptional thermal, mechanical and electrical properties.[1–5] Indeed, they have attracted considerable attention since they were first reported in 1991.[6] However, MWCNTs tend to aggregate into bundles due to van der Waals forces among MWCNTs, leading to poor dispersion of MWCNTs in aqueous solution, to further limit practical application of MWCNTs in various fields.[7] It therefore is a vital step to improve the effective dispersion and prevent the reaggregation of MWCNTs in solvents, enhancing their performance. Two approaches such as covalent modification through attaching molecules onto the backbone of MWCNTs[8] and non-covalent modification by adsorption of molecules onto the surface of MWCNTs,[9] have been widely applied to overcome this issue. As discussed so far, the covalent modifications proposed by researchers can efficiently introduce useful functional groups on the surface of MWCNTs. Nevertheless, this approach disrupts the sidewall structures of MWCNTs to alter their valuable properties.[10] In this regard, non-covalent functionalization is a promising way *via* the physical adsorption interaction between appropriate dispersing agents and MWCNTs.[11]

Up to now, MWCNTs are dispersed by non-covalent dispersion with the assistance of surfactants,[12] aromatic compounds,[13] and polymers.[14] Among the disperse progress of polymers, the stable suspend solution of MWCNTs complex can be formed between MWCNTs and polymer chains due to van der Waals interactions and π–π stacking. A high molar mass amphiphilic poly(styrene)-block-poly(2-vinylpyridine) (PS-BP2VP) was observed to perform an excellent dispersibility towards MWCNTs.[15] Meanwhile, polyoxyethylene (PEO) was adopted as an assistant phase to uniformly disperse MWCNTs.[16] Additionally, since it is better to develop MWCNTs for the potential use in both gas and liquid separation processes, homogeneous solution of MWCNTs can be obtained at the assistance of cellulose acetate (CA) in diacetone alcohol (DAA) solution.[17] On the other hand, biopolymer shows the dispersion ability towards MWCNTs. More

College of Science, Heilongjiang Bayi Agricultural University, Daqing, 163319, China. E-mail: gjlscl@sina.com

† Electronic supplementary information (ESI) available. See https://doi.org/10.1039/d2ra03592h

importantly, the prepared dispersible MWCNTs suspension in biopolymer media has a more important application values than those in other polymer media.[18] MWCNTs were dispersed by biopolymer carrageenan as a surfactant to subsequently form an excellent selectivity membrane for the removal of heavy metal ions from wastewater.[19] Unfortunately, among these applied polymers, they are widely used to disperse MWCNTs in organic phase, limiting their application in water phase.

Chitosan, a kind of natural polysaccharide, has been widely applied in various functional materials.[20–22] Recently, a series of bio-composites of chitosan/MWCNTs were investigated in some unique characteristics and applications.[23–25] It was reported that chitosan had the ability to disperse MWCNTs in the process of investigating dispersion behavior of MWCNTs.[26] Xu *et al.*[27] indicated that MWCNTs, being grafted with chitosan, were able to stably suspend in the solution. Nevertheless, a high molecular weight chitosan is poorly soluble in water due to intermolecular hydrogen bonding.[28] This is not beneficial for its utilization as a dispersant. In order to improve the dispersive ability of chitosan, wet-grinding assisted ultrasonication (GU) method was carried out in the process of investigating the dispersion behavior of MWCNTs in chitosan solution.[29] Furthermore, carboxymethyl chitosan, a derivative of chitosan, is easily soluble in water.[30] CMCS/MWCNT composites were prepared *via* covalent modification, possessing excellent solubility and stability both in DMSO and aqueous solution.[31]

Based on the above findings, here, to avoid to change the valuable electronic properties of oMWCNTs, we provided a method of dispersing oMWCNTs *via* non-covalent bond forces using a bio-composite *N*,*O*-carboxymethyl chitosan (*N*,*O*-CMCS) as a dispersant. This was expected to effectively disperse oMWCNTs in aqueous solution with exhibiting superior dispersion stability. Moreover, optical absorption spectroscopy was performed to illustrate the dispersion effect. In particular, FTIR spectrum, resonance Raman spectroscopy, and XRD patterns were performed to investigate the formation of a non-convalent interaction between *N*,*O*-CMCS and oMWCNTs. Additionally, cyclic voltammetry (CV) and electrochemical impedance spectroscopy (EIS) measurements were performed to investigate the electronic transmission ability of the dispersed oMWCNTs.

2 Experiments

2.1 Materials

MWCNTs (CVD, 90%, diameter 10–20 nm, length 10–20 μm) were provided by XFNANO China. Chitosan (Mn = 1.2 × 105 Da, deacetylation = 80%), chemicals such as isopropanol alcoholic solution, sodium hydroxide, monochloroacetic acid, ethanol, hydrochloric acid, and the iron detector solution were all of analytical purity and provided from Aladdin China. All dispersion experiments were carried out with distilled water.

2.2 Characterizations

Characterizations of the studied materials were identified using the flowing spectra. The Fourier transform-infrared (FTIR) spectra were recorded on a Fourier transform infrared spectrometer (Nicolet IS5) with a revolution of 4 cm^{-1} in the range of 400–4000 cm^{-1} using transmittance mode. UV-vis absorption spectra were recorded by a dual-beam spectrometer (UV3600, Shimadzu) operating with a spectral resolution of 0.2 nm between 200 and 800 nm. Transmission electron microscopy (TEM) observations of samples were carried out using a JEM 2100Plus at room temperature. Raman spectra were recorded by a micro laser Raman spectrometer (HR800, Jobin Yvon) excited with a helium laser at 633 nm at room temperature. Powder X-ray diffraction (XRD) patterns were obtained with a Rigaku D/max-IIIB diffractometer. The thermogravimetric analysis curves were performed using a differential scanning calorimeter (DSC, Netzsch STA 449C). X-ray photoelectron spectroscopy (XPS) patterns were obtained with a VG ESCALABMK II spectrometer. Cyclic voltammetry (CV) and electrochemical impedance spectroscopy (EIS) measurements were performed on electrochemical workstation (SP-300, BioLogic).

2.3 Preparation of water-soluble chitosan

As being illustrated in Fig. 1, *N*,*O*-carboxymethyl chitosan (*N*,*O*-CMCS) was prepared using previous methods.[32,33] Briefly, 10 g of chitosan was added to a 100 mL water/isopropanol alcoholic (1 : 4) solution in a reaction flask containing 10 g of NaOH. The dispersion progress was kept under magnetic stirring in water bath for 2 h at 283 K to make the chitosan alkalize and swell. Dissolved monochloroacetic acid (15 g) in 20 mL of isopropanol was thereafter slowly added to the reaction mixture. The progress was continuously proceeded at 283 K for 5 h to well complete the substitution reaction between chitosan and monochloroacetic acid. The suspension was subsequently filtered, and the precipitate was then washed with water/ethanol (1 : 1). Finally, a sodium salt of the water-soluble *N*,*O*-carboxymethyl chitosan was obtained. In order to obtain the acidic form of the water-soluble *N*,*O*-carboxymethyl chitosan, the sodium salt sample was suspended in 100 mL of 95% ethanol solution, and then a certain amount of 37% HCl was added under stirring for neutralization. The suspension was then filtered and the precipitate was washed with 95% ethanol subsequently dried under vacuum, the product of *N*,*O*-carboxymethyl chitosan named *N*,*O*-CMCS were obtained.

2.4 Oxidation of MWCNTs

HNO_3 treatment were used to oxidize and purify MWCNTs, as being previously established.[34] Briefly, 100 mg of MWCNTs was refluxed in 100 mL of 68 w/w% HNO_3 at 333 K for 5 h. Subsequently, the suspension liquid was placed to cool down, and then the clear solution on the top layer was decanted off. The

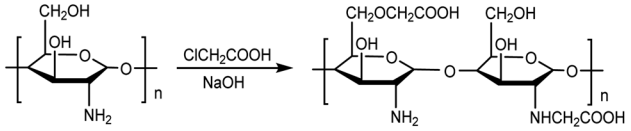

Fig. 1 Synthesis of water-soluble *N*,*O*-CMCS.

bottom layer MWCNTs were then filtered and washed with deionized water until attaining a neutral filtrate. Finally, the product was dried at 373 K in an oven for 2 h. The oxidized MWCNTs product was denoted as oMWCNTs.

2.5 Dispersion of oMWCNTs

The soluble *N*,*O*-CMCS/oMWCNTs composites were prepared as follows. 1.0 g of *N*,*O*-CMCS was dissolved in 100 mL deionized water and stirred for 10 minutes. Then, 10 mg of oMWCNTs was added to the solution for dispersing under ultrasonic treatment at 283 K for 1 h. The upper solution (80 v/v%) was collected after centrifugation at 3000 rpm, and the dispersed oMWCNTs were then filtered from the solution using a polytetrafluoroethylene filter with 0.45 μm. The dispersed oMWCNTs after filter, were washed thoroughly with distilled water to get rid of the extra *N*,*O*-CMCS, and then be dried at 333 K to obtain dispersible oMWCNTs in water. The final oMWCNTs blended with *N*,*O*-CMCS were denoted as *N*,*O*-CMCS/oMWCNTs composites.

3 Results and discussion

3.1 The formation of *N*,*O*-carboxymethyl chitosan

FTIR spectra were carried out to determine the carboxymethylation process and possible substitution site of carboxymethylation in CMCS, as being illustrated in Fig. 2a. For chitosan, a characteristic peak at 1650 cm^{-1} appeared, which could be attributed to the axial stretching of NH_2, and at 3291 cm^{-1} for the stretching vibration of –OH groups.[35] Compared to chitosan, two new bands of 1596 cm^{-1} and 1365 cm^{-1} were observed in the FTIR spectra of *N*,*O*-CMCS. These two bands were attributed to symmetric stretching of –C═O in $NHCH_2COOH$ and anti-symmetric stretching of –C═O in –COOH, respectively.[36] Furthermore, both C–O–C and –COOH stretching bands were observed at 1061 cm^{-1} and 3447 cm^{-1}, respectively.[30] The results of FTIR indicate that carboxymethylation process had occurred over –OH and $-NH_2$ groups of chitosan.[37] Theoretically, the introduced carboxyl effectively enhanced the hydrophilicity of chitosan, thus increasing absorptivity and dispersibility of *N*,*O*-CMCS.

To compare the crystallinity of chitosan and *N*,*O*-CMCS, their powder was analyzed using XRD, as being presented in Fig. 2b. For chitosan, two peaks of the maximum intensity remained at 26.2° and 72.9° (Fig. 2b-i), being matched with the values reported in previous report.[38] However, as being clearly shown in Fig. 2b-ii, these two peaks were significantly decreased at 26.2° and even disappeared at 72.9° after carrying out the analysis of carboxymethylation in *N*,*O*-CMCS. As being well documented, there were a large number of hydroxyl and amino groups in chitosan chains, leading to being associated with strong and regular hydrogen bonds. This was the main factor of the formation of crystalline regions in chitosan chains. Nevertheless, for *N*,*O*-CMCS, the decrease of crystallinity indicated that hydrogen bonds among chitosan chains were destroyed due to the introduction of carboxymethyl groups, further weaking intermolecular interaction among *N*,*O*-CMCS chains.[39] Here, we conclude that the original crystal structure of chitosan was destroyed and the *N*,*O*-CMCS was prepared successfully.

As being showed in Fig. 2c, TG spectra analysis was performed to investigate the thermostability of chitosan and *N*,*O*-

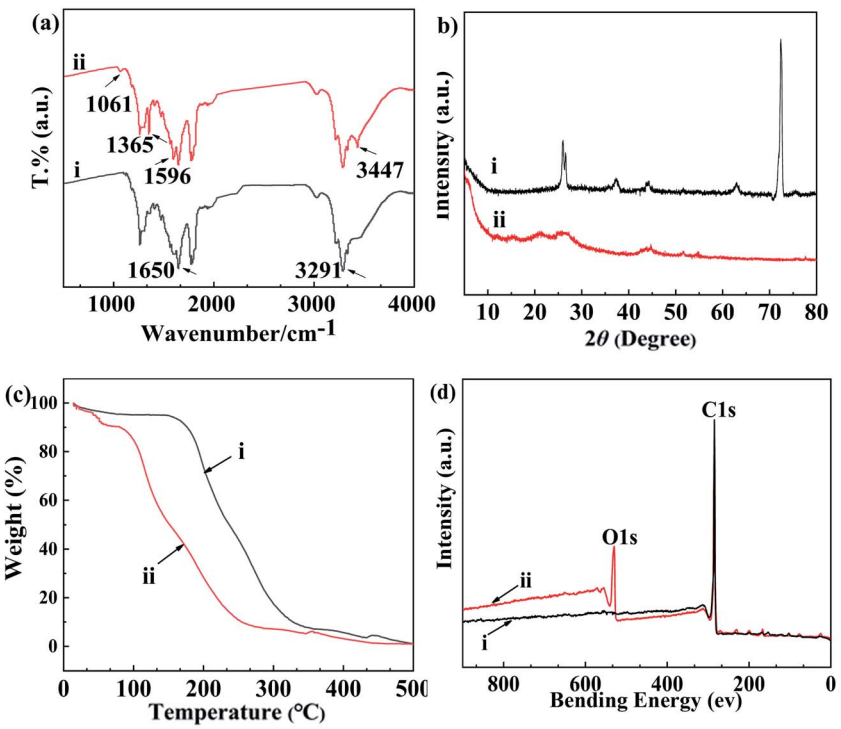

Fig. 2 FTIR spectra of (a-i) chitosan and (a-ii) *N*,*O*-CMCS; XRD patterns of (b-i) chitosan and (b-ii) *N*,*O*-CMCS; TGA thermograms of (c-i) chitosan and (c-ii) *N*,*O*-CMCS; Results of XPS analysis of (d-i) MWCNTs and (d-ii) oMWCNTs.

CMCS. The weight loss at the first stage was mainly related to the evaporation of adsorbed and bound water from 20–150 °C for chitosan in Fig. 2c–i but 20–120 °C for *N*,*O*-CMCS in Fig. 2c-ii.[40] In addition, the weight loss of chitosan and *N*,*O*-CMCS ranged from 5.7% to 11.2% at the first stage. Obviously, compared with chitosan, *N*,*O*-CMCS reflected greater weight loss at this stage with increasing hydrophilicity groups in *N*,*O*-CMCS chains. These results also further proved the introduction of carboxyl groups in *N*,*O*-CMCS *via* carboxymethylation progress.

The weight loss at the second stage started at about 150 °C and extended to 350 °C for chitosan but occurred in the temperature range of 120–300 °C for sample *N*,*O*-CMCS, where the weight loss of chitosan and *N*,*O*-CMCS stayed 76.4% and 85.1%, respectively. This weight loss was corresponded to the decomposition of the main chains of chitosan, the dehydration of saccharide rings, and cleavage of substituent groups in *N*,*O*-CMCS. As being observed in Fig. 2c, the thermal stability of *N*,*O*-CMCS was lower than that of chitosan, being similar with the previous study.[41]

3.2 The oxidation of MWCNTs

The existence of functional group attached on the surface of the MWCNTs could be indicated and identified by FTIR with the spectral range 400–4000 cm^{-1} (Fig. 2d). For MWCNTs, the peak at 1647 cm^{-1} (Fig. 2d–i) could be associated with the stretching of the backbone of MWCNTs.[42] Compared with the FTIR spectra of MWCNTs, the new bands at 2991 cm^{-1} and 3442 cm^{-1} were noticed at that of oMWCNTs (Fig. 2d-ii). The distinct band located at 2991 cm^{-1} could be associated to the stretching of C=O in –COOH, while the other bands at 3442 cm^{-1} could be assigned to the stretching of –OH in –COOH group.[43] The appearance of these two bands indicated that MWCNTs were successfully oxidized.

XPS analysis is a surface analytical and quantitative spectroscopic technique, which can examine the bonding state on the surface of MWCNTs before and after treatments.[44] The XPS analysis of MWCNTs and oMWCNTs are shown in Fig. S1.† There was only one major peak observed in the scan spectra because of the C1s photoelectron in Fig.S1a,† while in Fig.S2b,† a new peak due to the O1s photoelectron appeared, indicating that oxygen-containing functional groups were present on the surface of the oMWCNTs after acidification treatment.[45] Obviously, oxygen atoms were bound to oMWCNTs in the oxidation process, generating the carbonyl active sites on the surface of oMWCNTs, and thus, dispersant could easily bond to oMWCNTs *via* a non-covalent form in the subsequently dispersion process of oMWCNTs.[46]

3.3 The disperse ability of *N*,*O*-CMCS towards oMWCNTs

Fig. 3 shows the photographs of oMWCNTs dispersed in water and the aqueous solution of *N*,*O*-CMCS after the treatment of ultrasound for 10 min. It could be seen from Fig. 3a that black homogenous solution of oMWCNTs were formed with the assistance of *N*,*O*-CMCS. In sharp contrast, some black particles were visible in Fig. 3b. After setting for 30 days, the dispersion of

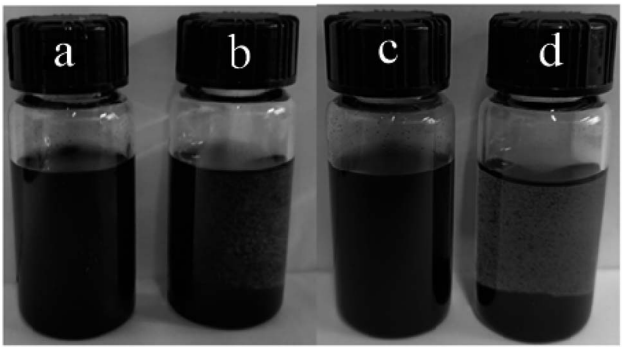

Fig. 3 Photographs of oMWCNTs dispersed (a) in water and (b) the aqueous solution of *N*,*O*-CMCS. (c) and (d) were taken after (a) and (b) setting for 30 days, respectively.

oMWCNTs dispersed with the *N*,*O*-CMCS showed a much strong stability (see Fig. 3c), whereas the oMWCNTs dispersed in water experienced serious agglomeration and precipitated completely (see Fig. 3d). It highlights that *N*,*O*-CMCS has a good dispersion ability towards oMWCNTs.

To better observe the micro morphological structure of oMWCNTs dispersed in water and *N*,*O*-CMCS, TEM investigation was performed. Fig. 4a presents the images of oMWCNTs, and fuzzy tubes were found due to other carbon impurities distributed among the bundles of oMWCNTs. In addition, some agglomerates were also found because of the van der Waals interaction (Fig. 4a). In contrast, TEM micrograph (Fig. 4b) clearly showed the well-isolated state of oMWCNTs with the dispersion treatment using *N*,*O*-CMCS, indicating that *N*,*O*-CMCS has a good ability to disperse oMWCNTs. After the ultrasonic dispersion treatment, the bundles were fully dispersed in soluble *N*,*O*-CMCS solution. Furthermore, both carbonaceous impurities and residual catalysts could be effectively removed *via* the centrifugation step, leaving mainly individually dissolved oMWCNTs in aqueous *N*,*O*-CMCS solution.

In the UV-vis region, well-dispersed MWCNTs could sharply display active sites, which was derived from the π–π transition of the C=C of individual MWCNTs.[47] Bundled MWCNTs, however, could not clearly be identified by the UV-vis spectra. This was because carries were tunneling among the bundled MWCNTs.[48] Therefore, the dispersion of MWCNTs could be performed with UV-vis absorption spectroscopy. The UV-vis absorption spectra of oMWCNTs and *N*,*O*-CMCS/oMWCNTs solubilized in water are shown in Fig. 5a. The UV-vis absorption spectra were recorded in the wavelength with the range from 200 to 800 nm. It was noticeable that the curve-*ii* exhibited an increased and broaden band attributed to oMWCNTs at 247 nm when the oMWCNTs was dispersed by *N*,*O*-CMCS, but the curve-*i* had a low intensity characteristic peak of oMWCNTs at 260 nm. Thereby, it could be concluded that the oMWCNTs was well dispersed with *N*,*O*-CMCS at the assistant of ultrasonic. Moreover, this peak downshifted from 260 nm to 247 nm after the *N*,*O*-CMCS attached onto the oMWCNTs, which was ascribed to the interaction between the *N*,*O*-CMCS and the oMWCNTs.[49] On the other hand, the van Hove singularities of

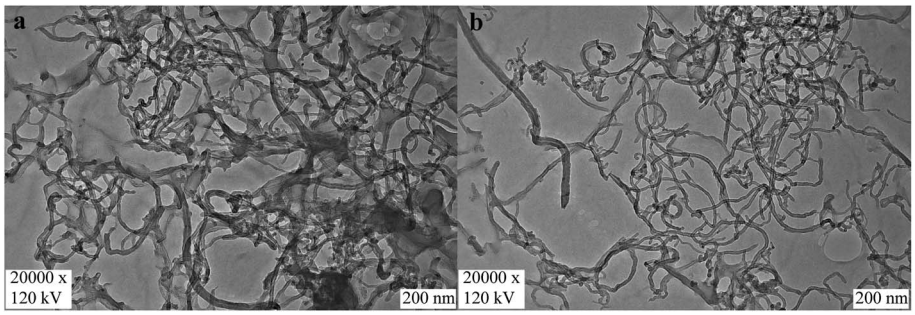

Fig. 4 TEM images of (a) oMWCNTs and (b) *N*,*O*-CMCS/oMWCNTs.

individual dispersed MWCNTs *via* chemical functionalization would remain, however, they would be sharply weakened.[50] It was observed that there were distinguishable and intense peaks in curve-*ii*. As a matter of fact, the curve-*ii* evidently exhibited more fine features than curve-*i* due to the van Hove transitions of essentially individual oMWCNTs.[51] It was worth to note that the van Hove singularities were not weakened but increased, which illustrated that the oMWCNTs were dispersed by *N*,*O*-CMCS *via* non-convert interaction.[50,51] Therefore, the UV-vis absorption spectra manifested that the oMWCNTs were fine individually dispersed in the aqueous solution of *N*,*O*-CMCS *via* non-convert interaction.

To investigate whether the dispersant of *N*,*O*-CMCS could decrease the electrochemical properties of oMWCNTs or not, cyclic voltammetry (CV) and electrochemical impedance spectroscopy (EIS) measurements were performed. The electrochemical properties of bare GCE, oMWCNTs modified electrode, and *N*,*O*-CMCS/oMWCNTs modified electrode were characterized by CV (Fig. S2†), respectively. In addition, the electrochemical properties of oMWCNTs modified electrode and *N*,*O*-CMCSoMWCNTs modified electrode were performed by EIS (Fig. S3†). The outcomes of CV and EIS demonstrated that *N*,*O*-CMCS/oMWCNTs showed an excellent capability to extend the active surface area and also increased the transfer of electrons between electrode and analyzed substances due to the disperse and synergistic effects of *N*,*O*-CMCS.[52] This provides an indirect support for the good dispersing ability of *N*,*O*-CMCS towards oMWCNTs. Furthermore, the electrical conductivity of

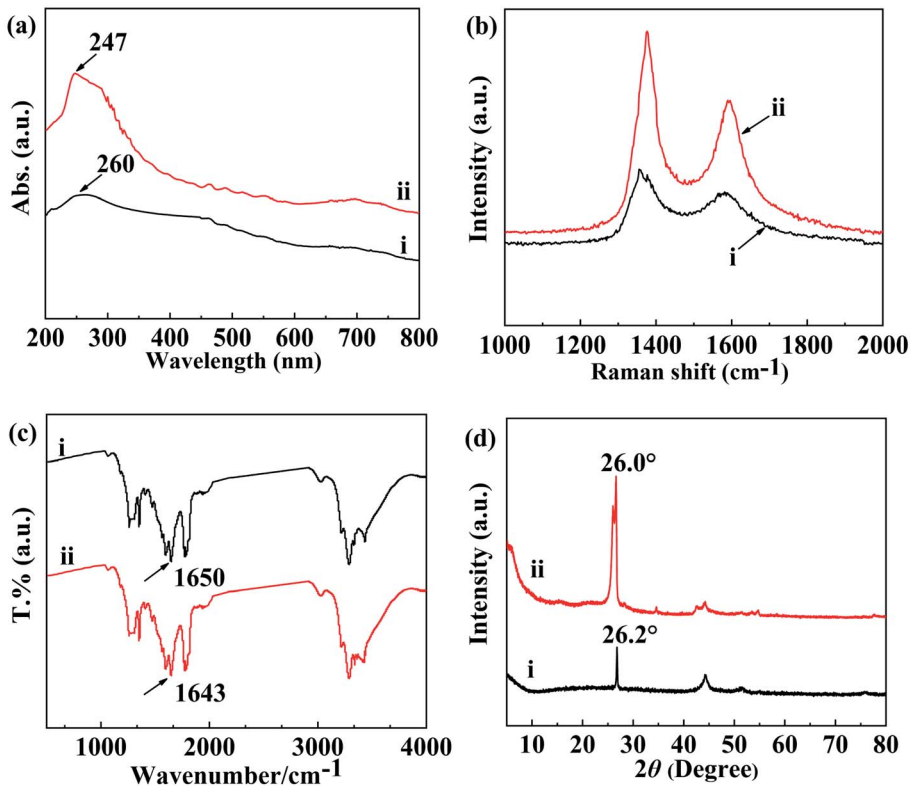

Fig. 5 UV-vis spectra of (a-i) oMWNTs and (a-ii) *N*,*O*-CMCS/oMWCNTs; Raman spectra of (b-i) oMWNTs and (b-ii) *N*,*O*-CMCS/oMWCNTs; FTIR spectra of (c-i) oMWNTs and (c-ii) *N*,*O*-CMCS/oMWCNTs; XRD patterns of (d-i) oMWCNTs and (d-ii) *N*,*O*-CMCS-oMWCNTs.

the dispersed oMWCNTs does not decrease but significantly increases due to the well-dispersed performance of *N*,*O*-CMCS. This study, therefore, also provides a novel *N*,*O*-CMCS/oMWCNTs composite for the design of electrochemical sensors.[53]

3.4 The non-covalent adsorption interaction between *N*,*O*-CMCS and oMWCNTs

The non-covalent adsorption interaction between organic molecules containing an electron-rich benzene ring and oMWCNTs was illustrated with an π–π electron donor–acceptor interaction, as being proposed by Shi *et al.*[54] In fact, oMWCNTs contained the both polarized electron rich and depleted sites, as it was primarily caused by the surface defects of oMWCNTs. Accordingly, a possible electron donor–acceptor interaction was that the *N*,*O*-CMCS ring electron-poor (n-electron acceptor) might have directly interacted with the electron-rich (π-electron donor) of oMWCNTs. To verify the n–π electron donor–acceptor mechanism for the non-covalent adsorption interaction between *N*,*O*-CMCS and oMWCNTs, the subsequent analysis was further carried out using Raman, FTIR and XRD spectra. Additionally, the p–π stacking between NH_2 groups in the *N*,*O*-CMCS chemical structure and SP^2–C in the surface of oMWCNTs might be another non-covalent adsorption interaction during the dispersion progress with an adsorbent. Finally, hydrogen bonding also played an important role during the adsorption progress of oMWCNTs.[55] Thus, the presence of –OH and –NH_2 groups in *N*,*O*-CMCS, results in the formation of hydrogen bonding with the –COOH group in oMWCNTs.

Indeed, Raman spectroscopy is a valuable tool for characterizing all graphite-like materials including MWCNTs. Raman spectra of MWCNTs showed two vibration peaks between 1000–2000 cm^{-1}. One strong band existed around 1580 cm^{-1} (G band) was attributed to the high-frequency E_{2g} first-order mode, and the other bands was attributed to the disorder-induced carbon remained around 1350 cm^{-1} (D band).[56] Meanwhile, the intensity ratio of the D and G band peaks (I_D/I_G) remained a parameter to assess the purity of MWCNTs, which was often used to evaluate the structural defects of MWCNTs.[57] Additionally, the larger the ratio is, the more the structural defects of MWCNTs are.

In this study, to better clarify the effect of the dispersion of *N*,*O*-CMCS towards oMWCNTs, resonant Raman spectroscopy was applied at the excitation wavelength of 633 nm. Fig. 5b shows the Raman spectra of oMWCNTs and *N*,*O*-CMCS/oMWCNTs at 633 nm. The I_D/I_G ratio of *N*,*O*-CMCS/oMWCNTs (1.42) in Fig. 5b-ii was a little higher than that of oMWCNTs (1.28) in Fig. 5b–i. This indicates that non group is covalently introduced on the surface of treated oMWCNTs, so the surface structure of oMWCNTs was not damaged by *N*,*O*-CMCS. On the contrary, it indicates that *N*,*O*-CMCS was adsorbed to the surface of MWCNTs by non-covalent interaction due to both of similar value of I_D/I_G.[58] As a result, this non-covalent adsorption improved the dispersibility of oMWCNTs in aqueous solution of *N*,*O*-CMCS, which was consistent with the result of UV–vis absorption spectra.

Moreover, according to Sergei Bronnikov *et al.*,[59] Raman spectroscopy could investigate the impact of charge transfer on the electronic structures of the doped MWCNTs[]. It could be seen from Fig. 5b that the D band upshifted from 1356 cm^{-1} for oMWNTs to 1375 cm^{-1} for *N*,*O*-CMCS/oMWCNTs. At the same time, compared with that of oMWCNTs, the G band of *N*,*O*-CMCS/oMWCNTs upshifted from 1587 cm^{-1} to 1596 cm^{-1}. Obviously, the upshift of the D and G band peaks was a result of the n–π electron donor–acceptor and hydrogen bonding interaction between the oMWCNTs and *N*,*O*-CMCS.[60]

FTIR spectroscopy was applied to investigate the charge transfer between *N*,*O*-CMCS and *N*,*O*-CMCS/oMWCNTs. Fig. 5c shows the FTIR spectra of (i) *N*,*O*-CMCS and (ii) *N*,*O*-CMCS/oMWCNTs. For *N*,*O*-CMCS, the band at 1650 cm^{-1} was ascribed to NH_2 group. After ultrasonication, NH_2 band for *N*,*O*-CMCS/oMWCNTs shifted towards to low frequency from 1650 to 1643 cm^{-1}. This result might be attributed to the strong interaction *via* p–π stacking between NH_2 groups in the *N*,*O*-CMCS chemical structure and SP^2–C in the surface of oMWCNTs.[61–64] On the other hand, it was probably derived from the change of hydrogen-bonding interaction of –COOH, –NH_2 or –OH groups in *N*,*O*-CMCS chains after being strong adsorbed on the surface of oMWCNTs.[60] Raman spectra analysis further indicates that the oMWCNTs bundles were disentangled with the dispersion proceeding of *N*,*O*-CMCS solution.

As shown in Fig. 5d, X-ray diffraction patterns of the oMWCNTs and *N*,*O*-CMCS/oMWCNTs were taken to reveal detailed information about the crystallographic structure of oMWCNTs. Three characteristic peaks of oMWCNTs at 26.2°, 43.1°, and 53.2° in curve-*i* were assigned to (002) graphite structure (100) and (004) diffraction planes, respectively, be in good agreement with previous report.[65] For *N*,*O*-CMCS/oMWCNTs, another new characteristic peak assigned to *N*,*O*-CMCS at 34.6° appeared in Fig. 5d-ii, indicating the formation of *N*,*O*-CMCS/oMWCNTs.[66] But the characteristic peak of oMWCNTs assigned to (002) graphite structure appeared at 26.0° without larger changes in Fig. 5d-ii. The similar XRD patterns of *N*,*O*-CMCS/oMWCNTs and oMWCNTs indicated that the *N*,*O*-CMCS/oMWCNTs still had the same cylinder wall structure as oMWCNTs. Thus, the structure of oMWCNTs was not destroyed even after the *N*,*O*-CMCS modification process, illustrating that the oMWCNTs were dispersed by *N*,*O*-CMCS *via* non-convert interaction. Furthermore, compared to that of oMWCNTs in Fig. 5d-i, a 0.2° downshift was observed at the XRD pattern of *N*,*O*-CMCS/oMWCNTs in Fig. 5d-ii, which originated from the non-covalent interaction between oMWCNTs and *N*,*O*-CMCS.[67] In addition, it was interesting to note that the intensity of a diffraction peak at (002) in *N*,*O*-CMCS/oMWCNTs was increased as compared with that of oMWCNTs, which was likely due to sample purification by *N*,*O*-CMCS dispersing progress.[68] This was in agreement with TEM analysis.

4 Conclusion

A water-soluble bio-composite *N*,*O*-CMCS, being synthesized with chitosan and monochloroacetic acid using the substitution reaction, showed an effective dispersion towards oMWCNTs

and prevented the reaggregation of oMWCNTs at the assistance of ultrasonic. The *N*,*O*-CMCS/oMWCNT dispersion solution maintained a superior dispersion stability for 30 days due to the physical adsorption of *N*,*O*-CMCS on the surface of oMWCNTs *via* a non-convert interaction. Uv–vis spectroscopic characterization confirmed that *N*,*O*-CMCS displayed an excellent dispersion towards oMWCNTs *via* a simple sonication and centrifugation process. Furthermore, Uv-vis, Raman, FTIR, and XRD spectra proved the charge interaction between oMWCNTs and *N*,*O*-CMCS, leading to the formation of the nonconvert complex between *N*,*O*-CMCS and oMWCNTs. Thus, oMWCNTs could be effectively dispersed with *N*,*O*-CMCS in aqueous solution *via* non-convert modifying based on n–π electron donor–acceptor, p–π charge stacking, and hydrogen-bonding interactions without damaging structures. Our findings indicate a great potential of *N*,*O*-CMCS as an effective dispersant in enhancing the dispersibility of oMWCNTs in aqueous solution. In addition, a novel *N*,*O*-CMCS/oMWCNTs composite is also provided due to its excellent electronic transmission capability for the design of electrochemical sensors.

Funding

This work was supported by the Natural Science Foundation of Heilongjiang Province of China (LH2019B012).

Conflicts of interest

No potential conflict of interest was reported by the authors.

Acknowledgements

This work was supported by the Talent Development Program in Heilongjiang Bayi Agricultural University (ZRCPY201818).

References

1 E. W. Wong, P. E. Sheehan and C. M. Lieber, *Science*, 1997, **277**(5334), 1971–1975.
2 E. Esmizadeh, A. Irani, G. Naderi, M. H. R. Ghoreishy and C. Dobious, *J. Appl. Polym. Sci.*, 2018, **135**(12), 45977.
3 H. Gu, H. Zhang, C. Ma, X. Xu, Y. Wang, Z. Wang, R. Wei, H. Liu, C. Liu, Q. Shao, X. Mai and Z. Guo, *Carbon*, 2019, **142**, 131–140.
4 S. O. Mirabootalebi, *Adv. Compos. Hybrid Mater.*, 2020, **3**(3), 336–343.
5 Z. Wang, X. Li, L. Wang, Y. Li, J. Qin, P. Xie, Y. Qu, K. Sun and R. Fan, *Adv. Compos. Hybrid Mater.*, 2020, **3**(1), 1–7.
6 S. Iijima, *Nature*, 1991, **354**(6348), 56–58.
7 S. Y. Wang, T. Song, H. S. Qi and Z. Y. Xiang, *Chem. Eng. J.*, 2021, **419**, 129602.
8 Z. C. Qu, K. X. Wang, C. A. Xu, Y. Li, E. X. Jiao, B. Chen, H. F. Meng, X. H. Cui, J. Shi and K. Wu, *Chem. Eng. J.*, 2021, **421**, 129729.
9 A. K. M. Moshiul Alam, M. D. H. Beg, R. M. Yunus and Q. T. H. Shubhrac, *Colloid Interface Sci. Commun.*, 2021, **42**, 100395.
10 R. Gupta and B. Singh, *Mater. Sci. Eng., B*, 2020, **262**, 114730.
11 E. Ortiz, P. Gallay, L. Galicia, M. Eguílaza and G. Rivasa, *Sens. Actuators, B*, 2019, **292**, 254–262.
12 M. Dobies, J. Iżykowska, M. Wilkowska, A. W. Braszak, K. Szutkowski, A. Skrzypczak, S. Jurga and M. Kozak, *J. Phys. Chem. C*, 2017, **121**(21), 11839–11850.
13 W. W. Xu, Q. W. Yin, Y. A. Gao and L. Yu, *Langmuir*, 2015, **31**(46), 12644–12652.
14 C. Pramanik, J. R. Gissinger, S. Kumar and H. Heinz, *ACS Nano*, 2017, **11**(12), 12805–12816.
15 M. M. L. Arras, B. He and K. D. Jandt, *Polymer*, 2017, **127**, 15–27.
16 T. Gong, M. Q. Liu, H. Liu, S. P. Peng, T. Li, R. Y. Bao, W. Yang, B. H. Xie, M. B. Yang and Z. H. Guo, *Polymer*, 2017, **110**, 1–11.
17 T. Esser, T. Wolf, T. Schubert, J. Benra, S. Forero, G. Maistros, S. Barbe, G. V. Theodorakopoulos, D. S. Karousos, A. A. Sapalidis and E. P. Favvas, *Nanomaterials*, 2021, **11**(2), 280.
18 A. A. Alshahrani, M. S. Algamdi, I. H. Alsohaimi, L. D. Nghiem, K. L. Tu, A. E. Al-Illwajfeh and M. I. H. Panhuis, *Sep. Purif. Technol.*, 2020, **234**, 116088.
19 A. Alshahrani, A. Alharbi, S. Alnasser, M. Almihdar, M. Alsuhybani and B. AlOtaibi, *Sep. Purif. Technol.*, 2021, **276**, 119300.
20 Y. Z. Pan, H. Q. Bao and L. Li, *ACS Appl. Mater. Interfaces*, 2011, **3**(12), 4819–4830.
21 M. A. Aroon, A. F. Ismail, M. M. Montazer-Rahmati and T. Matsuura, *J. Membr. Sci.*, 2010, **364**(1–2), 309–317.
22 J. Gao, M. Song, T. Li, Y. Zhao and A. Wang, *RSC Adv.*, 2022, **12**(11), 6821–6830.
23 Y. T. Ong, A. L. Ahmad, S. H. S. Zein, K. Sudesh and S. H. Tan, *Sep. Purif. Technol.*, 2011, **76**(3), 419–427.
24 C. Z. Thou, F. S. A. Khan, N. M. Mubarak, A. Ahmad, M. Khalid, P. Jagadish, R. Walvekar, E. C. Abdullah, S. Khan, M. Khan, S. Hussain, I. Ahmad and T. S. Algarni, *Arabian J. Chem.*, 2021, **14**(3), 103022.
25 L. A. Alshabanah, S. M. Gomha, L. A. Al-Mutabagani, T. Z. Abolibda, N. A. Abd El-Ghany, W. A. M. A. El-Enany, A. K. El-Ziaty, R. S. Ali and N. A. Mohamed, *Polymers*, 2021, **13**(11), 1728.
26 C. Iamsamai, S. Hannongbua, U. Ruktanonchai, A. Soottitantawat and S. T. Dubas, *Carbon*, 2010, **48**(1), 25–30.
27 Z. Gou, D. Xu, Q. Dong and X. Wu, *Starch-Stärke*, 2016, **68**(3–4), 220–229.
28 L. Pighinelli and M. Kucharska, *Carbohydr. Polym.*, 2013, **93**(1), 256–262.
29 C. Y. Tang, T. N. Zhou, J. H. Yang, Q. Zhang, F. Chen, Q. Fu and L. Yang, *Colloids Surf., B*, 2011, **86**(1), 189–197.
30 R. A. A. Muzzarelli, *Carbohydr. Polym.*, 2009, **76**(2), 167–182.
31 X. Hao, S. Chen, H. Yu, D. Liu and W. X. Sun, *RSC Adv.*, 2016, **6**(1), 39–43.
32 B. Doshi, E. Repo, J. P. Heiskanen, J. A. Sirviö and M. Sillanpää, *Carbohydr. Polym.*, 2017, **167**, 326–336.
33 R. G. M. A. Macedo, N. N. Marques, L. C. S. Paulucci, L. C. S. Paulucciaet, J. V. M. Cunha, M. A. Villetti,

B. B. Castroc and R. C. Balabana, *Carbohydr. Polym.*, 2019, **215**, 137–142.
34 K. Domagała, M. Borlaf, J. Traber, D. Kata and T. Graule, *Mater. Lett.*, 2019, **253**, 272–275.
35 D. K. Singh and A. R. Ray, *J. Appl. Polym. Sci.*, 1994, **53**(8), 1115–1121.
36 X. Zhao, K. Kato, Y. Fukumoto and K. Nakamae, *Int. J. Adhes. Adhes.*, 2001, **21**(3), 227–232.
37 M. Kaya, Y. S. Cakmak, T. Baran, M. Asan-Ozusaglam, A. Mentes and K. O. Tozak, *Biotechnol. Bioprocess Eng.*, 2014, **19**(1), 58–69.
38 N. K. Patel and V. K. Sinha, *Int. J. Polym. Mater.*, 2009, **58**(11), 548–560.
39 Y. Y. Yin, Q. F. Dang, C. S. Liu, J. Q. Yan, D. S. Cha, Z. Z. Yu, Y. C. Cao, Y. Wang and B. Fan, *Int. J. Biol. Macromol.*, 2017, **102**, 10–18.
40 A. L. Bukzem, R. Signini, D. M. Dos Santos, L. M. Lião and D. P. R. Ascheri, *Int. J. Biol. Macromol.*, 2016, **85**, 615–624.
41 P. D. Chethan, B. Vishalakshi, L. Sathish, K. Ananda and B. Poojary, *Int. J. Biol. Macromol.*, 2013, **59**, 158–164.
42 M. Morsy, M. Helal, M. El-Okr and M. Ibrahim, *Spectrochim. Acta, Part A*, 2014, **132**, 594–598.
43 B. Scheibe, E. Borowiak-Palen and R. J. Kalenczuk, *Mater. Charact.*, 2010, **61**(2), 185–191.
44 D. Xu, X. L. Tan, C. L. Chen and X. K. Wang, *J. Hazard. Mater.*, 2008, **154**(1–3), 407–416.
45 X. L. Ling, Y. Z. Wei, L. M. Zou and S. Xu, *Colloids Surf., A*, 2013, **421**, 9–15.
46 M. Bhaumik, S. Agarwal, V. K. Gupta and A. Maity, *J. Colloid Interface Sci.*, 2016, **470**, 257–267.
47 R. Rastogi, R. Kaushal, S. K. Tripathi, A. L. Sharma, I. Kaur and L. M. Bharadwaj, *J. Colloid Interface Sci.*, 2008, **328**(2), 421–428.
48 A. C. Zaman, F. Kaya and C. Kaya, *Ceram. Int.*, 2020, **46**(18), 29120–29129.
49 W. Feng, Y. Li and P. J. Ji, *AICHE J*, 2012, **58**(1), 285–291.
50 C. A. Dyke and J. M. Tour, *Nano Lett.*, 2003, **3**(9), 1215–1218.
51 T. P. Chua, M. Mariatti, A. Azizan and A. A. Rashid, *J. Alloys Compd.*, 2009, **480**(2), 534–536.
52 J. Zou, M. M. Yuan, Z. N. Huang, X. Q. Chen, X. Y. Jiang, F. P. Jiao, N. Zhou, Z. Zhou and J. G. Yu, *Mater. Sci. Eng.: C*, 2019, **103**, 109848.
53 S. Akbarzadeh, H. Khajehsharifi and S. Hajihosseini, *Biosensors*, 2022, **12**(7), 468.
54 W. K. Li, J. Chen, H. X. Zhang and Y. P. Shi, *Talanta*, 2017, **168**, 136–145.
55 W. K. Li, H. X. Zhang and Y. P. Shi, *Anal. Chim. Acta*, 2018, **1011**, 40–49.
56 E. F. Antunes, A. O. Lobo, E. J. Corat, V. J. Trava-Airoldi, A. A. Martin and C. Veríssimo, *Carbon*, 2006, **44**(11), 2202–2211.
57 V. L. Kuznetsov, S. N. Bokova-Sirosh, S. I. Moseenkov, A. V. Ishchenko, D. V. Krasnikov, M. A. Kazakova, A. I. Romanenko, E. N. Tkachev and E. D. Obraztsova, *Phys. Status Solidi B*, 2014, **251**(12), 2444–2450.
58 Y. L. Wang, W. C. Ji, Y. J. Xu, L. M. Zou, H. W. Lu and C. K. Sun, *Colloids Surf., A*, 2021, **608**, 125557.
59 S. Bronnikov, S. Kostromin, M. Asandulesa, D. Pankin and A. Podshivalov, *Compos. Sci. Technol.*, 2020, **190**, 108049.
60 U. Eduok, E. Ohaeri and J. Szpunar, *Electrochim. Acta*, 2018, **278**, 302–312.
61 D. Long, G. Wu and G. Zhu, *Int. J. Mol. Sci.*, 2008, **9**(2), 120–130.
62 F. Yao, W. Xie, M. Yang, H. Zhang, H. Gu, A. Du, N. Naik, D. P. Young, J. Lin and Z. Guo, *Mater. Today Phys.*, 2021, **21**, 100502.
63 J. Guo, Z. Chen, W. Abdul, J. Kong, M. A. Khan, D. P. Young, J. Zhu and Z. Guo, *Adv. Compos. Hybrid Mater.*, 2021, **4**(3), 534–542.
64 J. Gao, Y. Huang and Y. Lian, *RSC Adv.*, 2015, **5**(124), 102238–102246.
65 M. Bhaumik, S. Agarwal, V. K. Gupta and A. Maity, *J. Colloid Interface Sci.*, 2016, **470**, 257–267.
66 R. L. Patale and V. B. Patravale, *Carbohydr. Polym.*, 2011, **85**(1), 105–110.
67 X. P. Wei, Y. L. Luo, F. Xu, Y. S. Chen and L. H. Yang, *Mater. Des.*, 2016, **111**, 445–452.
68 M. Deborah, A. Jawahar, T. Mathavan, M. K. Dhas and A. M. F. Benial, *Spectrochim. Acta, Part A*, 2015, **139**, 138–144.